Theor Chem Acc (2009) 123:137–143
DOI 10.1007/s00214-009-0543-y

REGULAR ARTICLE

Long, multicenter bonding in π-[terthiophene]$_2^{2+}$ dimers

Iñigo Garcia Yoldi · Joel S. Miller · Juan J. Novoa

Received: 11 February 2009 / Accepted: 11 February 2009 / Published online: 5 March 2009

Abstract The repulsive nature of the interaction between the cation radicals of the π-[terthiophene]$_2^{2+}$ dimers, $\mathbf{1}_2^{2+}$, found in crystals has been concluded from B3LYP/6-31+G(d) calculations. Hence, the bonding component is weaker than the Coulombic repulsion, consistent to recent findings for $[TTF]^{\cdot+}$–$[TTF]^{\cdot+}$ interactions (TTF = tetrathiafulvalene). The existence of $\mathbf{1}_2^{2+}$ dimers originates from the cation$^+$–anion$^-$ electrostatic interactions, which exceeds the combined effect of the $\mathbf{1}^{\cdot+}$–$\mathbf{1}^{\cdot+}$ plus $(SbF_6)^-$–$(SbF_6)^-$ repulsions in $\mathbf{1}_2(SbF_6)_2$, similar to what is found for $[TTF]^{\cdot+}$–$[TTF]^{\cdot+}$ interactions in $[TTF]_2(ClO_4)_2$ aggregates and in crystals. The long, multicenter bond in $\mathbf{1}_2^{2+}$ is characterized as a $2e^-/10c$ bond from an Atoms-in-molecules analysis.

Dedicated to Professor Santiago Olivella on the occasion of his 65th birthday and published as part of the Olivella Festschrift Issue.

Electronic supplementary material The online version of this article (doi:10.1007/s00214-009-0543-y) contains supplementary material, which is available to authorized users.

I. G. Yoldi · J. J. Novoa (✉)
Departament de Química Física and IQTCUB Facultat de Química, Universitat de Barcelona,
Av. Diagonal, 647, 08028 Barcelona, Spain
e-mail: juan.novoa@ub.edu

J. S. Miller (✉)
Department of Chemistry,
University of Utah, Salt Lake City,
UT 84112-0850, USA
e-mail: jsmiller@chem.utah.edu

1 Introduction

Oligothiophenes [1] have been obtained and are model compounds for the study of polythiophenes [2]. In this context, the properties of π-dimers of oligomeric radical cations have attracted recent interest due to their relevance as an alternative to the presence of bipolarons in oxidized polythiophene [3, 4]. Recent EPR, UV–vis–NIR, and crystallographic data reveal the existence of these dimers in crystals and solution [5–7]. These π-dimers are detected in millimolar concentration at 180 K (a) due to new absorptions at 490, 762, and 1,080 nm, and (b) by a decrease in the intensity of the EPR signal due to a reduced population of a thermally populated triplet state, consistent with a diamagnetic nature of these π-dimers. The experimental study of the dimerization process gave thermodynamic parameters for the π-dimer formation of ΔH approximately -10 kcal/mol and ΔS approximately -25 eu [5].

The existence of these dimers in crystals and in solution is attributed [8, 9] to a weak chemical bonding between the two cation radicals that form the π-dimers. The weak chemical bonding was first established on the basis of theoretical calculations using local density (LDA) functionals [8], where the presence of a local metastable minimum for the dimer was found (the two fragments at 3.13 Å), although the minimum disappeared when using the more precise gradient corrected (GGA) functionals. More recently [9], based on crystallographic data, the presence of π-dimers in oxidized end-capped terthiophenes was demonstrated, Fig. 1. These dimers have interfragment C–C distances between the thiophene rings of 2.976 Å, i.e., shorter than the sum of the van der Waals radii of two C(sp^2) atoms (1.70 Å), a fact that prompted the authors to conclude that a strong attractive interaction operates between two terthiophenium radical cations end-capped by

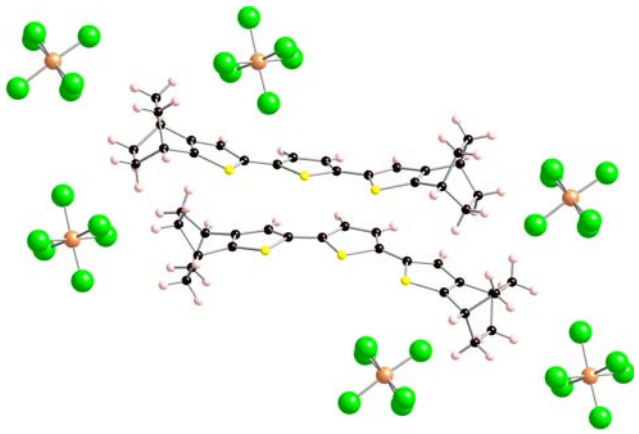

Fig. 1 Geometry of the π-$\mathbf{1}_2^{2+}$ dimers found in the **1**(SbF_6) crystal. C atoms are in *black*, S in *yellow*, Sb in *orange*, F in *green*, and H in *white*

bicyclo[2.2.2]octane units ($\mathbf{1}^{\cdot+}$). The authors took that fact "as a clear evidence that a π–π interaction can surpass the electrostatic repulsion and destabilization by structural deformation." The $\mathbf{1}^{\cdot+}$ cations form pairs where they bend toward the other, thus allowing the formation of short C–C and S–S contacts (the shortest ones being 2.976 and 3.650 Å, respectively). The existence of π-dimers of $\mathbf{1}^{\cdot+}$, π-$\mathbf{1}_2^{2+}$, was also reported for 1.2 mM solutions in CH_2Cl_2 at low temperature with an enthalpy of −6.7 kcal/mol.

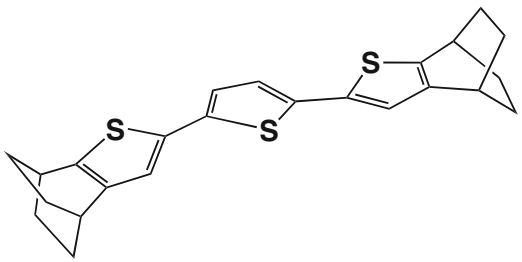

As already indicated, the intradimer interaction was attributed to weak chemical bonding stronger than the electrostatic repulsion [8, 9]. However, based on the recently reported understanding of the intradimer interactions for $[TTF]_2^{2+}$ [10], $\mathbf{1}_2^{2+}$ likely possesses long, multicenter intradimer bonding [11–14] (TTF = tetrathiafulvalene). In another words, although the $\mathbf{1}_2^{2+}$ dimers are not energetically stable when isolated, they form due to net stabilizing effect of their interaction with surrounding ions or solvent molecules [10–21]. Hence, we extend our theoretical studies on ion radical dimers to π-$\mathbf{1}_2^{2+}$ to gain a detailed understanding of the nature of the $\mathbf{1}^{\cdot+}$–$\mathbf{1}^{\cdot+}$ interaction, as well as the energetic considerations behind the presence of π-$\mathbf{1}_2^{2+}$ dimers in crystals. The results are particularly compared with those obtained for $[TTF]_2^{2+}$ observed in crystals [10], a prototype of cationic π-dimers with long, multicenter bonds.

2 Methodological details

Following the procedure used to study of the properties of $[TTF]_2^{2+}$ dimers [10], the characterization of the electronic structure and properties of π-$\mathbf{1}_2^{2+}$ dimers was executed in two consecutive steps. First, the interaction energy curve of an isolated π-$\mathbf{1}_2^{2+}$ dimer as a function of the shortest interfragment C–C distance was evaluated using the B3LYP density functional.[1] Then, the energetic interactions in the **1**[SbF_6] crystal preseting π-$\mathbf{1}_2^{2+}$ dimers was evaluated in order to identify the reasons behind the existence of these dimers in solids. The later energetic evaluation was done on the $\mathbf{1}_2^{2+}[SbF_6]_2$ aggregate, the smallest one where all the interactions found in the **1**[SbF_6] crystal are present. The results are then compared with those for $[TTF]_2^{2+}$ dimers found in $[TTF]_2(ClO_4)_2$ aggregates [10]. The large number of atoms of the π-$\mathbf{1}_2^{2+}$ dimers preempted the use of more sophisticate methods used in the study of the $[TTF]_2^{2+}$ dimers, such as the MCQDPT/CASSCF(2,2) method where one performs multiconfigurational perturbation calculation on a multiconfigurational CASSCF(2,2) wavefunction using the MCQDPT method [24, 25].[2] Although some of the features of the long bond in $[TTF]_2^{2+}$ require the use of the MCQDPT/CASSCF(2,2) method (the most relevant one being reproducing the equilibrium distance and diamagnetic nature of the ground state singlet), the B3LYP method can properly describe the SOMO–SOMO interaction and the Coulombic interaction, and it is thus sufficient to check which one is stronger. This will allow to identify the differences between the interactions in the π-$\mathbf{1}_2^{2+}$ and $[TTF]_2^{2+}$ dimers.

All B3LYP calculations were done using the 6-31+G(d) basis set [26] and the Gaussian-03 suite of programs [27]. Except when otherwise indicated, the interaction energies were corrected by the basis set superposition error using the counterpoise method [28–30].[3]

[1] B3LYP is a density functional obtained by taking the three parameter non-local exchange functional of Becke and the non-local correlation functional of Lee-Yang-Parr [22, 23].

[2] The MCQDPT/CASSCF(2,2) method performs multiconfigurational perturbation calculation on a multiconfigurational CASSCF(2,2) wavefunction using the MCQDPT method [24] provides an accurate evaluation of the dispersion component of the interaction energy and gives results similar to those obtained using the more popular CASPT2 method [25]. The (2,2) active space in these CASSCF(2,2), and MCQDPT/CASSCF(2,2) calculations was that resulting from combining the two SOMO orbitals of the fragments.

[3] The validity of the counterpoise method for correcting the BSSE was demonstrated analytically in Ref. [29] and numerically in Ref. [30].

3 Results and discussion

The SOMO and electronic spin distribution of a $\mathbf{1}^{\cdot+}$ and a $[TTF]^{\cdot+}$ monomer, computed at the UB3LYP/6-31+G(d) level, is shown in Fig. 2. Both monomers have a doublet ground state and have a π^* SOMO delocalized over the whole molecule (that for the $[TTF]^{\cdot+}$ is mostly localized on the central C–C atoms, while that for $\mathbf{1}^{\cdot+}$ is located only on the sp^2-C atoms of the five-membered rings, where the C=C double bonds are located in the neutral molecule **1**).

The potential energy curves for a $[TTF]_2^{2+}$ dimer computed at the RB3LYP/6-31+G(d) and UB3LYP/6-31+G(d) levels are shown in Fig. 3. The curves were obtained by optimizing the geometry of the dimer at each distance *d* (the shortest central C–C distance). It is clear that both curves are energetically unstable with respect to the dissociation of the dimer into its fragments; i.e. $[TTF]_2^{2+} \leftrightarrows 2\ [TTF]^{\cdot+}$. However, a very small metastable minimum is found in the RB3LYP curve, although it disappears when going into the UB3LYP curve after relaxing the doubly occupation restriction of the orbitals. The RB3LYP and UB3LYP curves can now be compared with those obtained at the MCQDPT/CASSCF(2,2) level [24, 25], Fig. 3, where a metastable minimum is found at ~3.2 Å (not found in CASSCF(2,2) calculations, thus indicating that the dispersion component of the interaction energy is qualitatively relevant). Consequently, in all three methods the formation of $[TTF]_2^{2+}$ is an endothermic and not spontaneous process (note, however, that the UB3LYP calculations do not predict a minimum while the RB3LYP and MCQDPT calculations both predict a metastable minimum). Hence, the formation of $[TTF]_2^{2+}$ is only possible when they are in an environment where they can get enough energy to compensate for the intrinsic energetic repulsive nature of their interaction. Thus, for $[TTF]_2^{2+}$ the bonding component of the interaction, which originates form the overlap of the two SOMO orbitals of the fragments, is less energetic than the Coulombic cation$^+$–cation$^+$ component originating from their net positive charges.

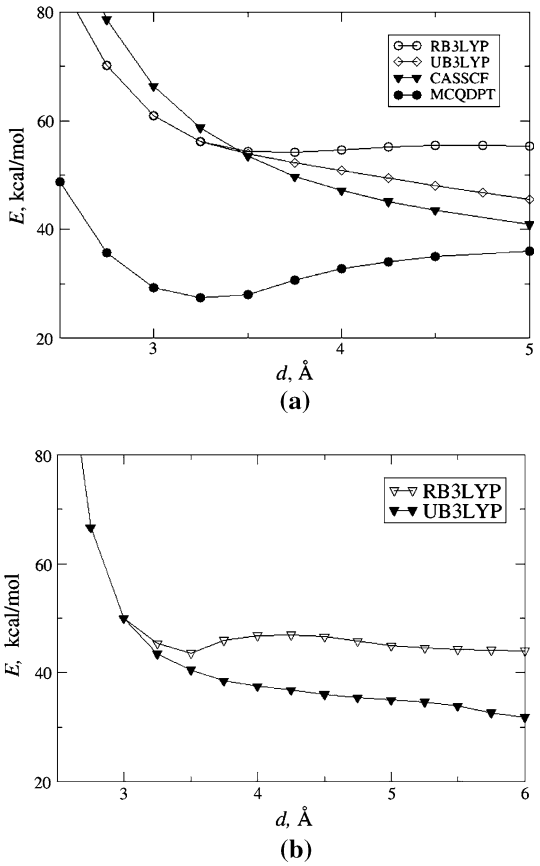

Fig. 3 **a** Variation of the interaction energy, *E*, of two $[TTF]^{\cdot+}$ fragments placed in a $D_{2\ h}$ geometrical arrangement as a function of interfragment C–C distance (*d*) computed at the RB3LYP and UB3LYP levels, as well as at the CASSCF(2,2) and MCQDPT/CASSCF(2,2) levels; **b** Variation of *E*, of two $\mathbf{1}^{\cdot+}$ fragments placed as in the crystal of $\mathbf{1}(SbF_6)$ (adapted from Ref. [9]), as a function of central interfragment C–C distance (*d*)

The potential energy curves for an isolated $\mathbf{1}_2^{2+}$ dimer computed at the RB3LYP/6-31+G(d) and UB3LYP/6-31+G(d) levels are also shown in Fig. 3. As in the $[TTF]_2^{2+}$ case, the RB3LYP curve presents a metastable minimum ~45 kcal/mol above the energy of two non-interacting

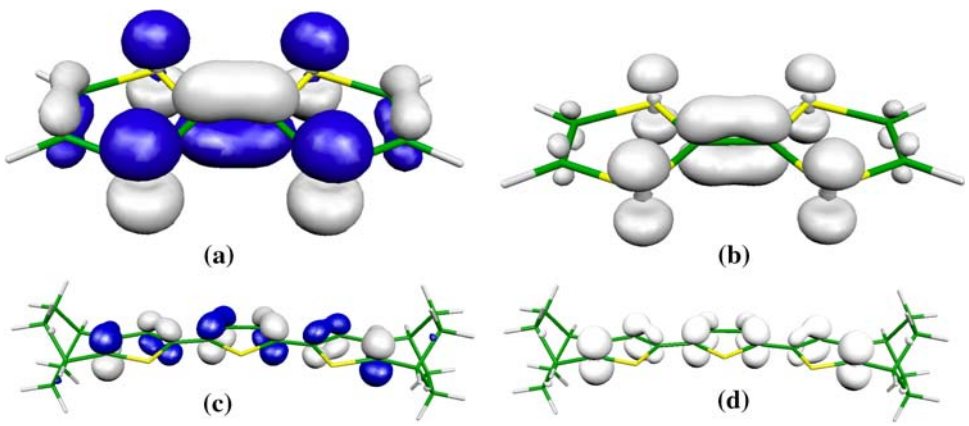

Fig. 2 **a** Shape of the SOMO of $[TTF]^{\cdot+}$; **b** shape of the spin density distribution of $[TTF]^{\cdot+}$; **c** shape of the SOMO if $\mathbf{1}^{\cdot+}$; **d** shape of the spin density distribution of $\mathbf{1}^{\cdot+}$; The atom color code is: S is *yellow*, C *green*, and H *white*, and the isosurface plotted is that of ±0.05 atomic units. All results were computed at the UB3LYP/6-31+G(d) level (note the absence of regions of negative electron density in both radicals at that isosurface)

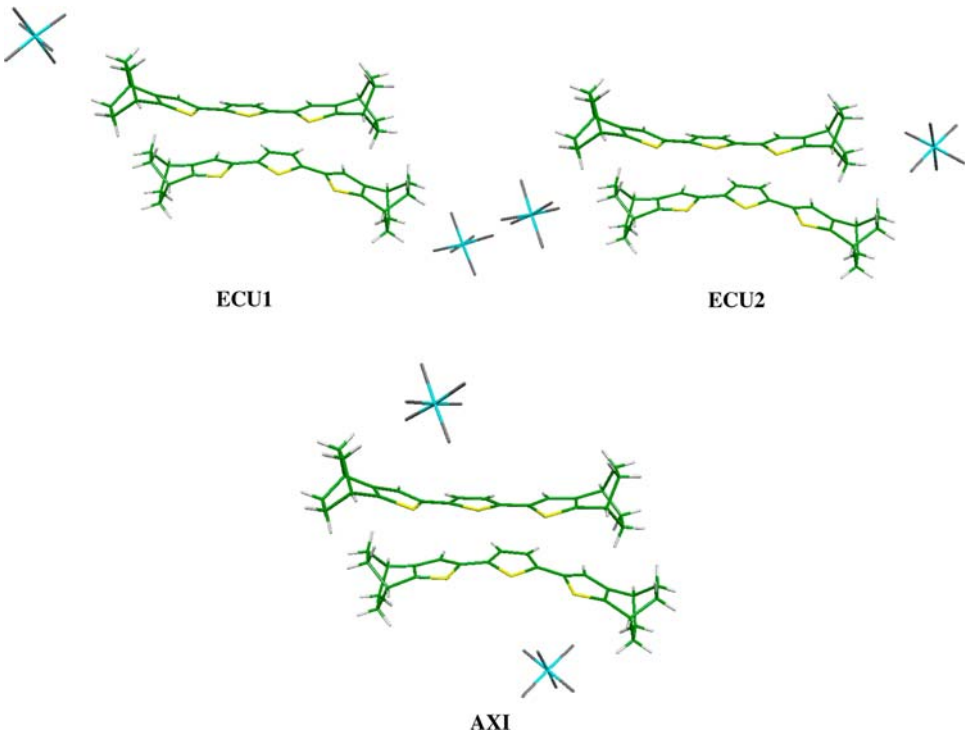

Fig. 4 Geometry of the ECU1, ECU2, and AXI aggregates built by selecting two opposite $(SbF_6)^-$ anions from the six nearest $(SbF_6)^-$ anions that surround any $\mathbf{1}_2^{2+}$ dimer in the $\mathbf{1}(SbF_6)$ crystal, Fig. 1. Atom color code: C are *green*, S are *yellow*, H are *white*, Sb are *blue*, and F are *gray*

fragments. This minimum disappears when the double occupancy condition is lifted, as in UB3LYP calculations. Although MCQDPT/CASSCF(2,2) calculations have not been done given the size of the system, a trend similar to that observed for $[TTF]_2^{2+}$ is expected. Therefore, as for $[TTF]_2^{2+}$, the bonding component of the interaction, which originates form the overlap of the two SOMO orbitals of the fragments, is less energetic than the Coulombic cation$^+$–cation$^+$ component originating from their net positive charges. Consequently, $\mathbf{1}_2^{2+}$ formation is only possible when their interactions with their surrounding species allows the formation of energetically stable aggregates where the intrinsic energetic repulsive nature of the $\mathbf{1}^{\cdot+}$–$\mathbf{1}^{\cdot+}$ interaction is overweighed by other attractive interactions. Therefore, the nature of the interactions in the isolated $\mathbf{1}_2^{2+}$ and $[TTF]_2^{2+}$ dimers are similar.

Since $\mathbf{1}_2^{2+}$ is not energetically stable, the nature of the $\mathbf{1}^{\cdot+}$–$\mathbf{1}^{\cdot+}$ interactions in crystals was sought. In $[TTF]_2^{2+}$ dimers, their existence in the solid was understood [10] to be a consequence of the existence of energetically stable $[TTF]_2(anion)_2$ aggregates that contain these dimers, being the stability of these aggregates originated in the cation$^+$–anion$^+$ attractive interactions, which exceeds the sum of the cation$^+$–cation$^+$ and anion$^-$–anion$^-$ repulsive interactions. This analysis is extended here to $\mathbf{1}_2^{2+}$ dimers.

The structure of the $\mathbf{1}_2(anion)_2$ aggregates was taken from the crystal structure of $\mathbf{1}(SbF_6)$, Supplementary Figure 1 [9]. $\mathbf{1}(SbF_6)$ consists of *ac* planes where each $\mathbf{1}_2^{2+}$ dimer is surrounded within the plane by four anions. These planes are stacked in a way that adjacent ones are slightly shifted. As a result, the $\mathbf{1}_2^{2+}$ dimers are surrounded by four $(SbF_6)^-$ anions in the plane and by one $(SbF_6)^-$ anion in each of the two adjacent planes (Fig. 1). Nearby $\mathbf{1}_2^{2+}$ dimers in the same *ac* plane are separated by anions. The shortest contacts among these dimers between adjacent planes are made either between the central part of one dimer and the hydrogens of the end-capping units, or between two end-capping units. In these conditions, the SOMO orbitals of adjacent $\mathbf{1}_2^{2+}$ dimers present a negligible overlap.

Using as initial geometry the $\mathbf{1}_2^{2+}$ dimer and its six nearest $(SbF_6)^-$ anions, three different symmetric neutral $\mathbf{1}_2(SbF_6)_2$ aggregates can be identified, i.e., ECU1, ECU2, and AXI, Fig. 4. These differ in the relative position of the two anions. Two of them, ECU1 and ECU2, have their $(SbF_6)^-$ anions in equatorial positions, and the remaining one, AXI, have their anions in distorted axial positions. The ECU1 geometry is computed to be the most stable of the three aggregates for the closed-shell singlet, open-shell singlet, and triplet states, Table 1, and only the ECU1 aggregate will be discussed further. Interestingly, the UB3LYP result is always slightly more stable than the RB3LYP-computed interaction energy (the occupation number for the two orbitals that originate from combining the SOMOs of the two fragments is 1.97 and 0.03; in good agreement for the occupation of these two orbitals for $[TTF]_2^{2+}$ computed at the UB3LYP level [1.93 and 0.07], while that computed at the CASSCF(2,2) is 1.69 and 0.31

Table 1 Interaction energy, E, of the three aggregates of Fig. 4 relative to their dissociation into its four constituent fragments at the geometry of these fragments in the crystal

Aggregate	E(CSS)	E(OSS)	E(triplet)
ECU1	−84.8	−85.7	−80.0
ECU2	−77.7	−78.6	−73.6
AXI	−64.0	−64.1	−58.4

For each aggregate, the energy for the singlet state computed at the RB3LYP level (closed-shell singlet state, CSS), and UB3LYP level (open-shell singlet state, OSS), and for the triplet state (UB3LYP) are given

electrons). Hence, the UB3LYP method shows a mixture of closed-shell/open-shell characters found at the CASSCF(2,2) level for the $[TTF]_2^{2+}$ singlet ground state, and was used for $\mathbf{1}_2^{2+}$, although such mixture is smaller at the UB3LYP level.

E for the singlet and triplet states of ECU1 is always negative (−85.7 kcal/mol at the UB3LYP/6-31+G(d) level), indicating the energetic stability of this aggregates against the dissociation into its four constituent fragments at the crystal geometry (the same is also true for all other aggregates in Table 1). These values can be compared with the −147.2 kcal/mol UB3LYP/6-31+G(d) interaction energy for the most stable $[TTF]_2[ClO_4]_2$ aggregate [10], which is also energetically stable against dissociation into its four constituent fragments.

By comparing the most important, first-neighbor pair calculations for the $[TTF]_2[ClO_4]_2$ and $\mathbf{1}_2[SbF_6]_2$ aggregates, the origin of their stability can be rationalized. The most relevant first-neighbor pair interactions are the cation$^+$–cation$^+$ and anion$^-$–anion$^-$ interactions, and the four cation$^+$–anion$^-$ interactions, Fig. 5. Looking at their values, the origin of the stability of the $[TTF]_2(ClO_4)_2$ aggregate from the B3LYP calculations can be traced to the cation$^+$–anion$^-$ interactions, after comparing the sum of the cation$^+$–cation$^+$ (63.5 kcal/mol) and anion$^-$–anion$^-$ (29.6 kcal/mol) repulsions with the sum of the cation$^+$–anion$^-$ attractions (−255.8 kcal/mol, which results from adding the following four components: −64.3, −63.3, −60.0, and −68.2) [10].[4] The stability of the $\mathbf{1}_2(SbF_6)_2$ aggregate from B3LYP calculations also originates form the cation$^+$–anion$^-$ interactions: the cation$^+$–cation$^+$ and anion$^-$–anion$^-$ interactions are both repulsive (by 53.2 and 12.9 kcal/mol), while the cation$^+$–anion$^-$ interactions are all attractive (−41.2, −41.3, −31.2, and −32.7 kcal/mol and totals −146.4 kcal/mol). That is, the pair interactions

[4] The closed-shell singlet state of the $[TTF]_2(ClO_4)_2$ aggregate was also found to be −19.7 kcal/mol more stable than its fragmentation into two $[TTF]^+$ and two $(ClO_4)^-$ ions at the crystal geometry (the open-shell singlet and triplet states are also more stable than the fragments by −19.6 and −6.8 kcal/mol, respectively).

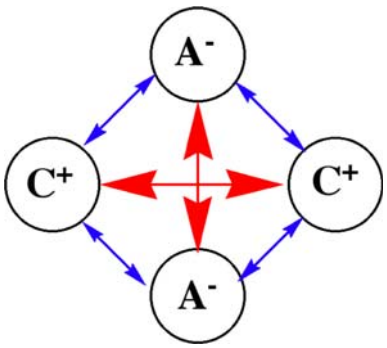

Fig. 5 Schematic representation of the most important, first-neighbor pair interactions in the $\mathbf{1}_2(anion)_2$ and $[TTF]_2(anion)_2$ aggregates. Cations are indicated as C^+ and anion as A^-

predict the $[TTF]_2(ClO_4)_2$ and the $\mathbf{1}_2(SbF_6)_2$ aggregate to be stable by −162.7 and −80.3 kcal/mol, with both values being very close to the reported interaction energy of −147.2 [10] and −85.7 kcal/mol (an indication of the goodness of the qualitative pair analysis). The pair analysis also indicates that the reduced stability of $\mathbf{1}_2(SbF)_2$ with respect to $[TTF]_2(ClO_4)_2$ can be associated to a weaker cation$^+$–anion$^-$ interactions (−146.4 kcal/mol versus −255.8 kcal/mol), as the sum of the cation$^+$–cation$^+$ and anion$^-$–anion$^-$ repulsions in the second aggregate (93.1 kcal/mol) is weaker than that in the first one (by 66.1 kcal/mol). Therefore, the presence of $\mathbf{1}_2^{2+}$ in the $\mathbf{1}_2(SbF)_2$ aggregates obeys the same rules found before on other pairs of ion radicals [10–18]. Consequently, one can safely conclude that $\mathbf{1}^{2+}$ possesses long bonds, as has been established for other ion radical pairs [10–18].

One can now look at the properties of the long bond in $\mathbf{1}^{2+}$. For such a task, the electronic properties of the cation$^+$–cation$^+$ interactions for $\mathbf{1}_2(SbF_6)_2$ was analyzed at its crystal geometry (Fig. 1). Despite the long interfragment C–C distances (3.090, 3.274, and 3.275 Å are the shortest three interfragment C–C distances), and despite the repulsive character of the $\mathbf{1}^{\cdot+}$–$\mathbf{1}^{\cdot+}$ interaction, the HOMO and LUMO orbitals of the aggregate originate from the bonding and antibonding combinations of the two $\mathbf{1}^{\cdot+}$ SOMO orbitals, Fig. 6. This shows that the electronic structure of the $\mathbf{1}^{\cdot+}$–$\mathbf{1}^{\cdot+}$ interaction follows the same principles already observed in the $[TTF]^{\cdot+}$–$[TTF]^{\cdot+}$ interactions, and are also found in other long bonded ion radical dimers: due mostly to the stabilizing effect of the cation$^+$–anion$^-$ interactions (and, as in the $[TTF]^{\cdot+}$–$[TTF]^{\cdot+}$ interactions, probably helped by the dispersion component), the two $\mathbf{1}^{\cdot+}$ SOMOs are forced to overlap and the resulting molecular orbital diagram presents all the features of a conventional covalent bond. An Atoms-in-molecules (AIM) analysis [31] of the RB3LYP wavefunction provided additional information with respect to the nature of the intradimer long bond in $\mathbf{1}_2^{2+}$. From the location in the electron density of the (3,−1)

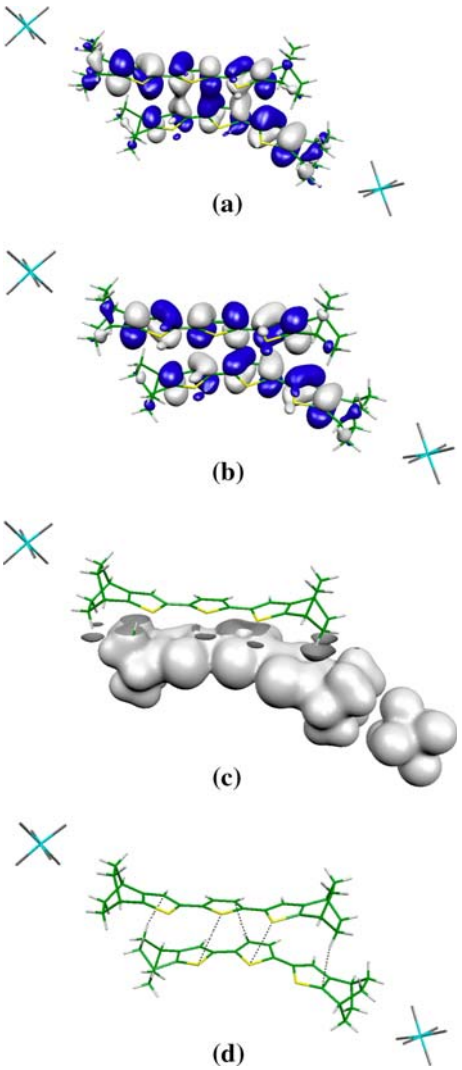

Fig. 6 HOMO (**a**) and LUMO (**b**) of the $[1]_2(SbF_6)_2$ aggregate computed at the UB3LYP/6-31+G(d) level; **c** electron density and **d** bond critical points found in a AIM analysis (adapted from Ref. [31]) of the UB3LYP electron density of the same aggregate. The geometry of the $[1]_2(SbF_6)_2$ aggregate is taken directly form the crystal. The color code is the same used in Fig. 4

bond critical points [31] that connect atoms within the $\mathbf{1}_2^{2+}$ dimer, the $\mathbf{1}^{+}$–$\mathbf{1}^{\cdot+}$ long bond involves two electrons and five overlaps, or five bonding component (Fig. 6d): one C–C, two S–S, and two C-H···C bonding components. The electron density of these points are: 12.4×10^{-3} (C–C), 7.6×10^{-3} (the two S–S) and 7.4×10^{-3} atomic units (the two C-H···C). The Laplacian for these five bond critical points is negative. Hence, the $\mathbf{1}_2^{2+}$ dimer has a long, $2e^{-}$/10c bond. By comparison, the long, multicenter bond in the $[TTF]_2^{2+}$ in $[TTF]_2(ClO_4)_2$ involves two electrons and eight bonding components (four C–C and four S–S) and is a $2e^{-}$/16c long bond.

Finally, let us point that due to the large size of $\mathbf{1}_2^{2+}$, MCQDPT/CASSCF(2,2) calculations on the $\mathbf{1}_2(SbF_6)_2$ aggregate were not executed. However, when these computations were done on the much smaller $[TTF]_2(ClO_4)_2$ aggregate, it confirmed the energetic stability found at the UB3LYP level. The main difference between the MCQDPT/CASSCF(2,2) and UB3LYP results was that the optimum geometry at the UB3LYP level is found at interfragment separations that are too long compared to the experimental results, a fact that is corrected by the MCQDPT/CASSCF(2,2) calculations, and the closed-shell nature of the singlet ground state not properly reproduced by the UB3LYP calculations that predict an open-shell singlet as ground state. However, these two results do not affect the attractive or repulsive nature of the $\mathbf{1}^{\cdot+}$–$\mathbf{1}^{\cdot+}$ interactions, and of the presence of long, multicenter bonds between them.

4 Conclusion

The repulsive nature of the interaction between the two cation radicals of the π-$[terthiophene]_2^{2+}$ found in crystals has been shown from B3LYP/6-31+G(d) calculations. This repulsive character shows that in these dimers the bonding component (π–π interaction or other authors [9]) is weaker than the Coulombic repulsion, similar to that recently reported for $[TTF]^{\cdot+}$–$[TTF]^{\cdot+}$ interactions, considered as a good prototype for the interaction between two cation radicals.

It has also been shown that the short intradimer distance dimers in $[1]_2(SbF_6)_2$ originates from the $cation^{+}$–$anion^{-}$ electrostatic interactions, which exceeds the combined effect of the $\mathbf{1}^{\cdot+}$–$\mathbf{1}^{\cdot+}$ plus $(SbF_6)^{-}$–$(SbF_6)^{-}$ repulsions. This is similar to that found in $[TTF]_2(ClO_4)_2$ [10] when comparing the sum of the $[TTF]^{\cdot+}$–$[TTF]^{\cdot+}$ and $anion^{-}$–$anion^{-}$ repulsions with the addition of the $cation^{+}$–$anion^{-}$ attractive interactions. Thus, a long, multicenter bond is present within the $\mathbf{1}_2^{2+}$ dimers. From an AIM analysis, it is characterized as a $2e^{-}$/10c long bond.

Acknowledgments I.G. Yoldi and J.J. Novoa were supported by the Spanish Science and Education Ministry (BQU2002-04587-C02-02 and UNBA05-33-001, and Ph.D. grant to I.G. Yoldi) and the CIRIT (2001SGR-0044 and 2005-PEIR-0051/69). Computer time was also provided by CESCA and BSC. J.S. Miller was supported in part by the U. S. NSF (Grant No. 0553573), and the DOE (Grant No. DE FG 03-93ER45504). One of us would also express here his gratitude to Prof. S. Olivella for his guidance, support, and personal friendship in the early years of his scientific career.

References

1. Hotta S, Waragai K (1993) Adv Mater 5:896. doi:10.1002/adma.19930051204

2. Nalwa HS (ed) (1997) Handbook of organic conductive molecules and polymers. Wiley, New York
3. Chang AC, Miller LL (1987) Synth Met 22:71
4. Zinger B, Mann KR, Hill MG, Miller LL (1992) Chem Mater 4:1113. doi:10.1021/cm00023a033
5. Hill MG, Mann KR, Miller LL, Penneau JF (1992) J Am Chem Soc 114:2728. doi:10.1021/ja00033a063
6. Miller LL, Yu Y, Gunic E, Duan R (1995) Adv Mater 7:547. doi:10.1002/adma.19950070606
7. Graf DD, Miller LL, Mann KR (1996) J Am Chem Soc 118:5480. doi:10.1021/ja960194b
8. Brocks G (2000) J Chem Phys 112:5353. doi:10.1063/1.481105
9. Yamazaki D, Nishinaga T, Tanino N, Komatsu K (2006) J Am Chem Soc 128:14470. doi:10.1021/ja065995l
10. Garcia-Yoldi I, Miller JS, Novoa JJ (2009) J Phys Chem A (in press)
11. Novoa JJ, Lafuente P, Del Sesto RE, Miller JS (2001) Angew Chem Int Ed 40:2540
12. Novoa JJ, Lafuente P, Del Sesto RE, Miller JS (2002) Angew Chem Int Ed 4:373
13. Del Sesto RE, Miller JS, Lafuente P, Novoa JJ (2002) Chem Eur J 8:4894
14. Miller JS, Novoa JJ (2007) Acc Chem Res 40:189
15. Novoa JJ, Ribas-Ariño J, Shum WW, Miller JS (2007) Inorg Chem 46:103
16. Garcia-Yoldi I, Mota F, Novoa JJ (2007) J Comput Chem 28:326
17. Garcia-Yoldi I, Miller JS, Novoa JJ (2007) J Phys Chem A 111:8020
18. Garcia-Yoldi I, Miller JS, Novoa JJ (2008) Phys Chem Chem Phys 10:4106
19. Lu J-M, Rosokha SV, Kochi JK (2003) J Am Chem Soc 125:12161
20. Jakowski J, Simons J (2003) J Am Chem Soc 125:16089
21. Jung Y, Head-Gordon M (2004) Phys Chem Chem Phys 6:2008
22. Becke AD (1993) J Chem Phys 98:5648
23. Lee C, Yang W, Parr RG (1988) Phys Rev B 37:785
24. Nakano H, Nakayama K, Hirao K, Dupuis M (1997) J Chem Phys 106:4912. doi:10.1063/1.473540
25. Roos BO, Andersson K, Fulscher MK, Malmqvist PA, Serrano-Andres L, Pierloot K, Merchan M (1996) Adv Chem Phys 93:219. doi:10.1002/9780470141526.ch5
26. Ditchfield R, Hehre WJ, Pople JA (1971) J Chem Phys 54:724
27. Frisch MJ et al (2004) Gaussian-03, Revision-C.02. Gaussian Inc., Wallingford
28. Boys SF, Bernardi F (1970) Mol Phys 19:553. doi:10.1080/00268977000101561
29. van Duijneveldt FB, de Rijdt JGCM, van Lenthe JH (1994) Chem Rev 94:1873. doi:10.1021/cr00031a007
30. Novoa JJ, Planas M, Whangbo MH (1994) Chem Phys Lett 225:240. doi:10.1016/0009-2614(94)00646-6
31. Bader RF (1990) Atoms in molecules. A quantum theory, Clarendon Press, Oxford